JTTEE5 16:768–775
DOI: 10.1007/s11666-007-9132-6
1059-9630/$19.00 © ASM International 2007

Fabrication of Functionally Graded SOFC by APS

Y.Z. Yang, H.O. Zhang, G.L. Wang, and W.S. Xia

(Submitted March 3, 2007; in revised form June 6, 2007)

Atmospheric plasma spray (APS) was used to prepare the planar positive/electrolyte/negative (PEN) and mono-block layer built (MOLB) type PEN solid oxide fuel cells (SOFCs). On the basis of the spraying conditions optimized previously and the self-developed functionally graded powder feeder system, two types of PEN cells were fabricated. Then the microstructure and material composition of the PEN cells were analyzed. The results show that graded layers formed between the electrodes and electrolyte. Moreover, the material composition and the porosity of the graded layers vary gradually. In particular, the porosities of the resultant anode and cathode reach 32.74 and 32.24%, respectively. Using the AC complex impedance technique, the conductivity of the MOLB type composite electrode is tested. The electrical conductivity of the MOLB type composite electrode with the graded layers is larger than that without the graded layers.

Keywords atmospheric plasma spray, electrical conductivity, functionally graded layers, PEN, SOFC

1. Introduction

The solid oxide fuel cell (SOFC) has drawn keen attention because of its high energy efficiency, low environmental hazards, high power density, and excellent integration with a simple reformer. Thus, SOFC is expected to realize commercialization within a few years and be a promising candidate for future energy conversion systems in the 21st century (Ref 1-3). However, the status of the development is still at a moderate level, and some key technical issues have not been resolved yet.

Generally, intermediate-temperature SOFCs operate under high-temperature conditions (~600 to 1000 °C). The strict bonding among each cell component results in mechanical constraints; thus a slight mismatch in the coefficient of thermal expansion (CTE) of cell components causes large thermal stress (Ref 4). As a consequence, CTE matching among the cell components is indispensable to reduce the internal stress. In addition, the contact state of the interfaces between electrodes and electrolyte severely influences the output power of the SOFC. Therefore, it is important to improve the interface bonding and to avoid the segregation and breakage caused by thermal expansion under cyclic high-temperature conditions.

Functionally graded materials (FGMs) provide a solution for many advanced applications, where two or many kinds of materials with distinct properties are required to be integrated together. Therefore, FGMs have received interest and have been applied in a wide range of applications, such as navigation industry, nuclear power source, electrical material, chemical industry, and so forth (Ref 5-7). Recently, the theory of FGM has also been used in SOFCs to effectively release the mismatch in the CTE and improve the interface bonding.

In FGM research, how to fabricate the parts with FGM is one of the most important areas. In the past, a huge spectrum of processing methods to prepare the FGM had been reported (Ref 8-12), including centrifugal separation method, powder metallurgy, hot pressing, sintering, and atmospheric plasma spray (APS) (Ref 13-20). Due to its wide range of spraying material, flexibility, and low cost, APS is the most commonly employed among these methods. However. Little information is available about fabricating functionally graded positive/electrolyte/negatives (PENs) for SOFC application.

In this paper, a new three-hopper powder feeding device was designed and developed for transporting many kinds of powders with different feeding rates at same time. The functionally graded planar and mono-block layer built (MOLB) type PEN cells were manufactured by APS. Then the microstructure and the material composition of the resultant PEN cells were investigated and analyzed. Finally, the electrical conductivity of the MOLB type composite electrode with and without the graded layers

This article is an invited paper selected from presentations at the 2007 International Thermal Spray Conference and has been expanded from the original presentation. It is simultaneously published in *Global Coating Solutions, Proceedings of the 2007 International Thermal Spray Conference*, Beijing, China, May 14-16, 2007, Basil R. Marple, Margaret M. Hyland, Yuk-Chiu Lau, Chang-Jiu Li, Rogerio S. Lima, and Ghislain Montavon, Ed., ASM International, Materials Park, OH, 2007.

Y.Z. Yang, G.L. Wang, and **W.S. Xia**, State Key Laboratory of Material Processing and Die & Mould Technology, Huazhong University of Science & Technology, Wuhan 430074, P.R. China; and **H.O. Zhang**, State Key Laboratory of Digital Equipment and Manufacturing Technology, Huazhong University of Science & Technology, Wuhan 430074, P.R. China. Contact e-mail: zholab@mail.hust.edu.cn.

were tested and compared using the (alternating current (AC) complex impedance technique. On the basis of the Arrhenius equation, the influence of temperature on the electrical conductivities was also analyzed.

2. Experimental

2.1 Powder Feeding Device and Design of FGM Component

During fabrication of the functionally graded PEN, a three-hopper powder feeding device was applied to feed two or more kinds of powders into the plasma torch (Ref 21). Figure 1 illustrates the principle sketch and photograph of the device. During spraying, the piston driven by the stepper motor moves accurately and transports the powder into the cavity. The powder is dispersed by the flexible brush and then is penetrated into the plasma jet with the help of the carrier gas N_2.

Powder feeding rate and its uniformity directly influence the material composition and proportion of the layers, which influences the mechanical and physical-chemical performances of the PEN cell. So the feeding rate of the three hoppers needed to be controlled precisely and be adjusted sensitively. For the device shown in Fig. 1, the powder feeding rate of every hopper was determined by:

$$m = (\rho \times n \times P \times \pi \times R^2 \times t)/i \quad \text{(Eq 1)}$$

where m is powder feed mass, ρ is density of powder, n is rotation speed of stepper motor, P is the screw pitch, R is radius of steel bushing, and i is velocity ratio coefficient of worm and gear. During the preparation process, n is the only adjustable parameter during spraying. Therefore, the powder feeding rate is determined by the rotating velocity of the stepper motor (n). On the basis of the calibration experiments, the relationship between the powder feeding rate and the rotating velocity of the stepper motor is shown in Fig. 2.

The functionally graded PEN presented in this paper contained two additional graded layers between the electrodes and electrolyte, which differs from the traditional PEN with only three layers. The graded layer (PE) was prepared between the anode and the electrolyte, and another layer (EN) was prepared between the electrolyte and the cathode. To gradually change the material components and the performance of the graded layers, the PE and EN layers were divided into 15 sublayers (PE1 to PE15, EN1 to EN15). Each sublayer was presettled with different spraying conditions illustrated in Fig. 3. During the preparation of the graded layers, two powder hoppers worked simultaneously, and two kinds of SOFC materials were provided according to the different mixture ratio to meet with the requirements of the graded PEN design.

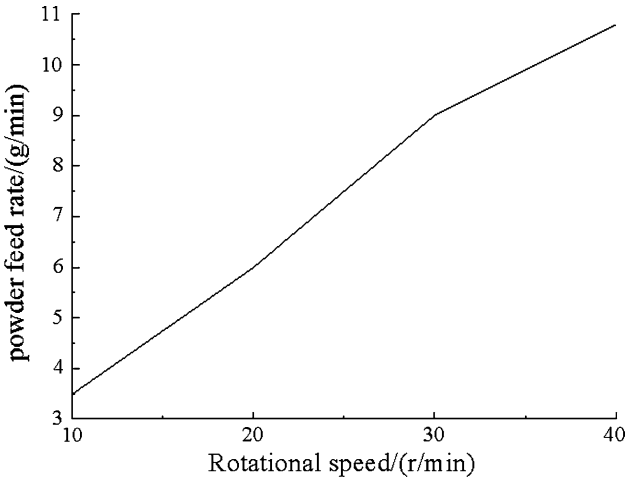

Fig. 2 Variation of the powder feed speed versus the rotation speed of the electric stepper motor

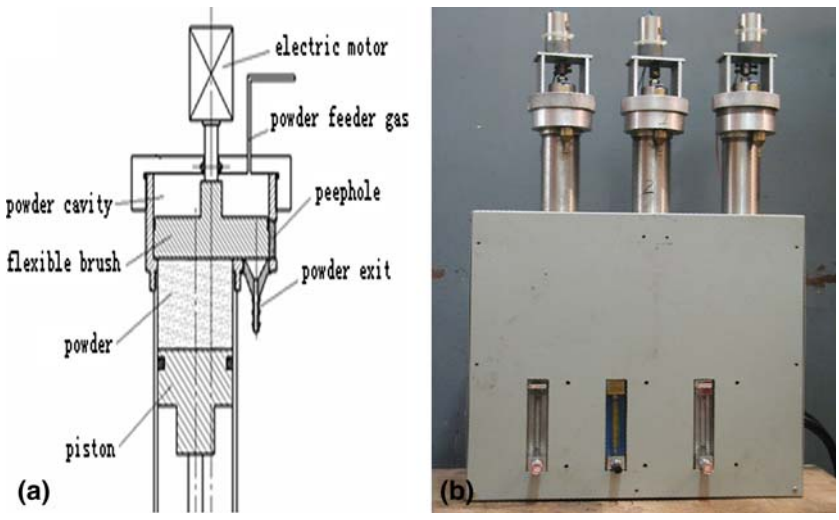

Fig. 1 The principle sketch (a) and photograph (b) of the three-hopper powder feed device

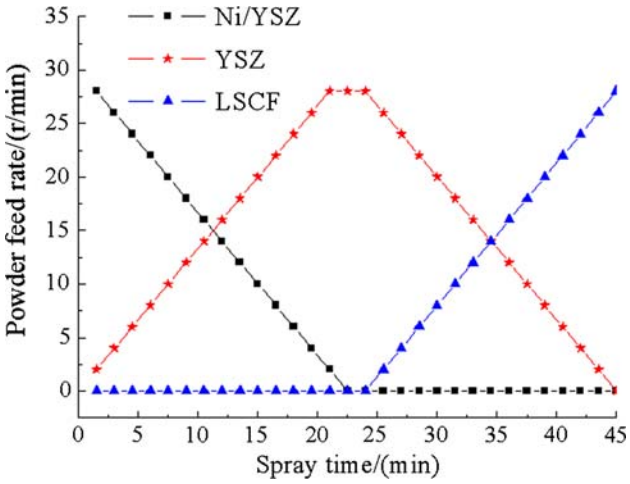

Fig. 3 Powder feed rate and spraying time of the graded layers

2.2 Preparation of Material

Commercial 8YSZ (8 mol% yttria-stabilized zirconia oxide, WIENER Corp., China) and Ni (WIENER Corp., China) (45 vol.%) powders were mixed for the starting anode material. A quantity of carbon powder was added to the starting anode material to increase the porosity of the anode. The powder mixture after ball milling for 24 h was dried at 80 °C in a baking oven and then crushed. The powder mixed with polyvinyl alcohol was screened and heated at 160 °C in an insulated box for 3 h to make it suitable for APS. Then the particle dimension distribution was adjusted to the range of 90 to ~120 μm for good flowability.

Commercial WIENER 8YSZ powder, which has a primary particle size of ~1.97 to 18.07 μm within a granule, was also ball milled and crushed by the same preparation means of the anode material mentioned previously. Then the particle dimension distribution was adjusted to the range of ~70 to 100 μm prior to deposition of the electrolyte coating.

Considering the good chemical-thermal stability and high electric conductivity, $La_{0.8}Sr_{0.2}Co_{0.5}Fe_{0.5}O_3$ primary powder was prepared via the sol-gel route for the cathode powder. Firstly, the stable solution was formed, mixing the $LaNO_3$ (lanthanum nitrate) solution, $SrNO_3$ (strontium nitrate) solution, $Co(NO_3)_2$ (cobalt nitrate) solution, and $Fe(NO_3)_3$ (ferrum nitrate) solution according to the stoichiometric proportion. After the solution flowed inversely for ~2 to 3 h at 80 °C and evaporated on a thermal plate, a homogeneous sol formed that was then heated to form the gel. The gel was calcined in a specific stove for 2 h and crushed to form the $La_{0.8}Sr_{0.2}Co_{0.5}Fe_{0.5}O_3$ primary powder. To improve the flowability of the powder, the $La_{0.8}Sr_{0.2}Co_{0.5}Fe_{0.5}O_3$ primary powder was also screened and heated at 160 °C in an insulated box for 3 h. Finally, the particle dimension distribution was adjusted to in the range of ~90 to 120 μm.

Fig. 4 The CAD model of the corrugation type PEN prototype

Table 1 Processing parameters of the PEN fabricated by APS

	Power, kW	Interval, mm	Spray angle, degrees	*t*, min
Ni + YSZ8	28	12	65	48
Graded layer	36	11/10	75 to 82	20
YSZ	39	10	90	30
Graded layer	36	10/11	82 to 75	20
LSCF	32	10	65	40

2.3 Preparation of PEN

Mild steel plates (Q235) of size 100 by 110 by 4 mm^3 were selected as substrates. They were previously grit blasted and cleaned in acetone prior to spraying. The grit-blasting material was corundum with the particle size of 83 to 840 μm, and the other conditions included gas pressure of 6.5 MPa and distance of (120 mm. Other ceramic substrates of size 120 by 80 by 15 mm^3 were also used. Experimental trails were carried out with a Metco 9MB gun (Sulzer Metco Corporation supplied in China) under ambient atmosphere.

Some major plasma spraying parameters, such as plasma power, powder feeding rate, spray angle, robot scanning step, velocity, and so on, significantly influence the microstructure of as-sprayed coatings, which in turn determines the catalytic activity and ionic conductivity of all three components of PEN. These parameters also influence the uniformity of the temperature and stress distribution during the coating deposition, which determine the microstructure of the PEN SOFC. In particular, the spray angle severely influences the porosity of the electrodes. Generally, the porosity increases with the decreasing of the spray angle, which is measured between the axis of spray gun and the sprayed plane. So the APS parameters must be optimized to process the cell component material into the desired macrostructure and favorable microstructure. On the basis of the simulation and experimental results (Ref 22-23), the spray parameters were optimized and are listed in Table 1.

The geometry model of the PEN is described in Fig. 4. Figure 5 shows the flowchart of the PEN preparation used for this paper; the functionally graded PEN was separated from the substrate using the grinding method (see Fig. 6).

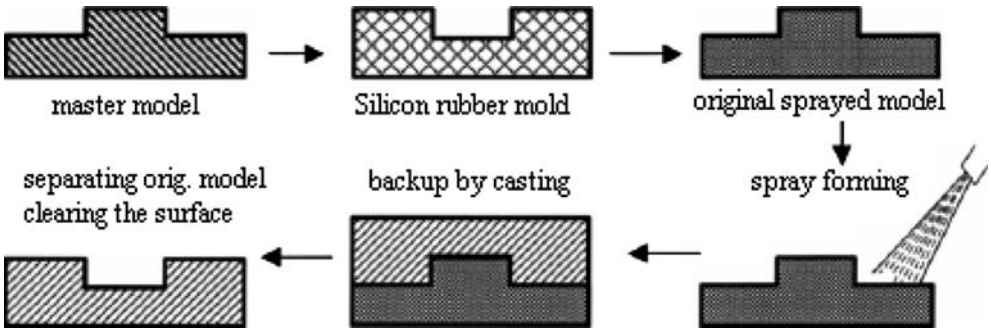

Fig. 5 The flowchart of rapid preparation of PEN by plasma spraying

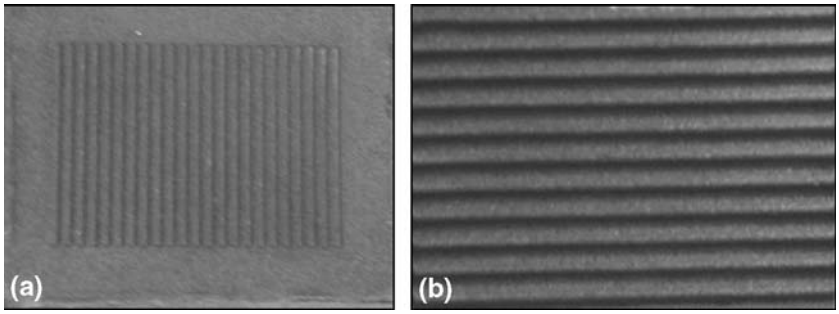

Fig. 6 Photograph of the ceramic prototype (a) and the PEN before separating from the ceramic substrate (b)

3. Results and Discussion

3.1 Material Composition and Microstructure Analysis of PEN

Using the electron probe microanalyzer (EPMA-1600, JINDAO International Trade Corp., Japan), the material elements and microstructure of the PEN were analyzed qualitatively and quantitatively. Figure 7 illustrates the surface line-scan photograph of the planar and MOLB type PEN coatings, respectively. The PENs are composed of anode, graded layer, electrolyte, graded layer, and cathode. In the two graded layers between the electrodes and the electrolyte, the material compositions gradually vary. The porosity of the PE graded layer changes gradually from high to low, and the porosity of the electrolyte is less than 3%. However, the porosity of the EN graded layer gradually changes from low to high. The thicknesses of the anode, the electrolyte, and the cathode are 200, 60, and 100 μm, respectively. To prevent increasing the resistance of cell, the graded layer is only ~20 to 30 μm thick.

According to the energy spectral analysis, four kinds of material elements (La, Sr, Fe, Co) are observed in the cathode layer, two kinds of elements (Y, Zr) are in the electrolyte layer, and three kinds of elements (Y, Zr, Ni) are in the anode layer, as shown in Fig. 8. Moreover, the material composition in the PE and EN layers gradually change according to the element distribution in graded layers, so the performances of the graded layers may gradually change. As a result, the mismatch of the thermal expansion between the electrodes and electrolyte is released, which must decrease the possibility of the cracking.

Generally, the anode and the cathode layers of the PEN need to be highly porous for better fuel/oxygen permeability and catalytic activity, but the electrolyte layer needs to be fully dense and thin. Using the Quanta 200-type Environmental Scanning Electron Microscopy (ESEM; FEI Corp., USA), SEM (secondary electron) micrographs of the anode, the electrolyte, and the cathode were made (Fig. 9). The electrolyte layer exhibited a dense lamellar microstructure, and the electrolyte porosity was less than 3%. The anode and the cathode layers were obviously porous, as shown in Fig. 9(b) and (c). Moreover, using the image analysis method, porosity of the anode and the cathode was tested and reached 32.7 and 32.4%, respectively.

3.2 AC Complex Impedance Analyses

Alternating current complex impedance measurement was carried out to test the resistance of the two kinds of composite electrodes, one of which consisted of the cathode, EN graded layer, and the electrolyte, and the other consisted of the cathode and the electrolyte. The resistance included the grain resistance (R_g), intergrain resistance (R_{gb}), and the interface contact resistance between components of the composite electrode (R_{ct}) (Ref 24-25). The corresponding ideal AC complex impedance plots (Cole-Cole half circle) and the equivalent circuit are

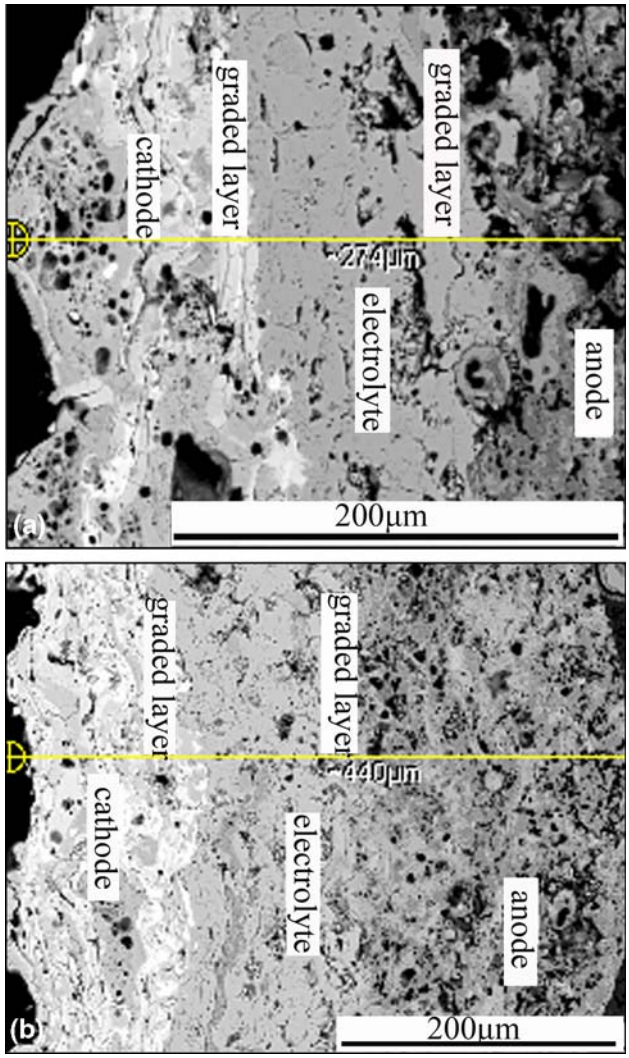

Fig. 7 Photographs of surface linear scan of the planar PEN (a) and the MOLB type PEN (b)

shown in Fig. 10. According to the Cole-Cole half circle, the resistances were defined as:

$$Z' = R_g + R_{gb} + R_{ct} \quad \varpi \to 0$$
$$Z' = R_g \quad \varpi \to \infty \qquad \text{(Eq 2)}$$

On the basis of the intercept of the Cole-Cole half circle on the Z' axle, the grain resistance, intergrain resistance, and the interface contact resistance were obtained.

The AC impedance device (VMP/2, Princeton Applied Research Corp., USA) and the two-electrode method were applied to test the electrical conductivity of the composite electrodes. In the AC complex impedance testing, Pt slurry, of the area of which was 5 mm diameter, was coated on the electrolyte and electrode layer. Pt wire was welded to contact with the Pt slurry areas, and then the pigtail of the Pt wire contacted with the AC impedance tester. Under the air and nitrogen environment, the complex impedance of composite electrodes was tested. Some AC complex impedance plots were obtained by increasing the testing temperature from 500 to 800 °C and changing the test frequency in the range of ~10 to 200 MHz.

In general, the electrical conductivity of the composite electrode varies with temperature. The variation relation between the electrical conductivity and temperature is described by:

$$\sigma = \sigma_0 \exp\left(-\frac{E_a}{KT}\right) \qquad \text{(Eq 3)}$$

where σ is electrical conductivity, σ_0 is conductivity constant, E_a is electric conduction activation energy of material, K is Boltzmann constant, and T is testing temperature.

Figures 11 and 12 show the AC complex impedance plots of the two kinds of the composite electrodes. As can be seen, the grain resistance and the interface resistance of the composite electrodes decrease with the increase in

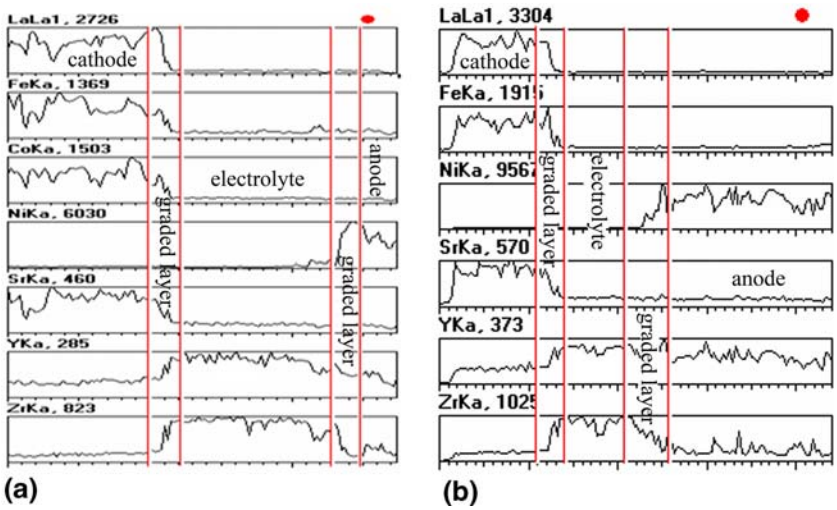

Fig. 8 Element energy spectrum of the planar PEN (a) and the MOLB type PEN (b)

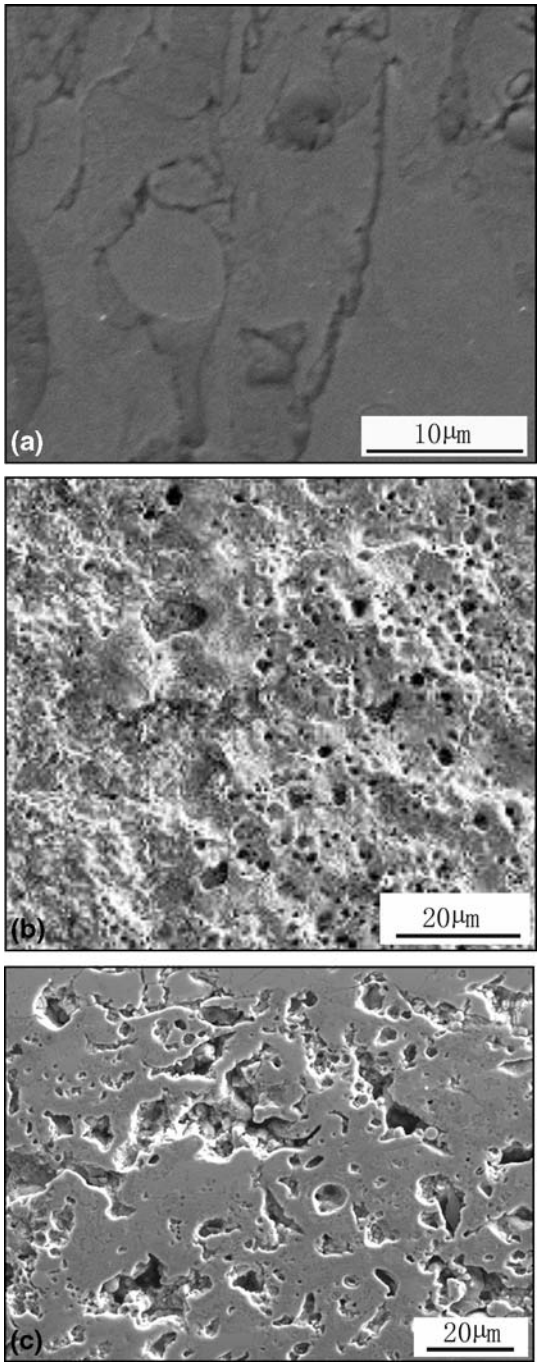

Fig. 9 Scanning electron micrographs of the electrolyte (a), the anode (b) and the cathode (c) of the MOLB type PEN

temperature; namely, the negative temperature coefficient (NTC) effects of composite electrodes appeared.

To investigate the variation of the resistance with temperature quantitatively, Eq 2 was used to analyze the testing results shown in Fig. 11 and 12, and the Arrhenius curves (ln σ - 1/*T*) of electrical conductivity and temperature were obtained.

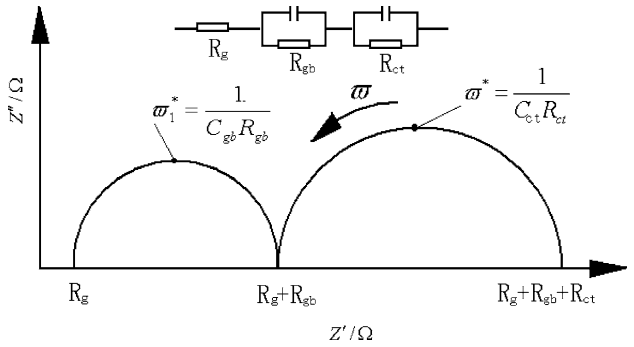

Fig. 10 Ideal AC complex impedance plots and the equivalent circuit diagram

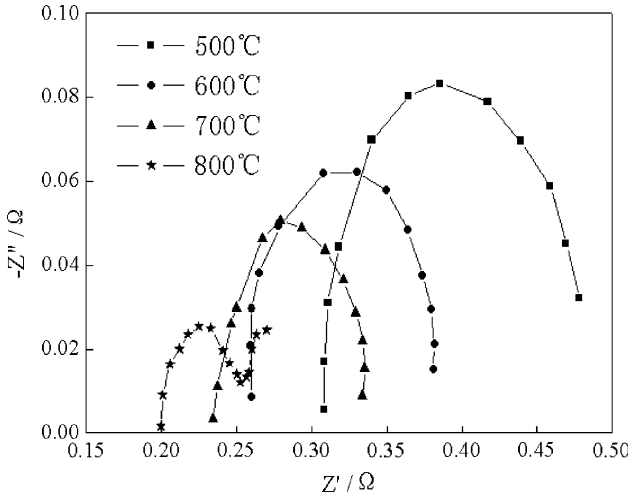

Fig. 11 AC complex impedance plots of the PEN with the graded layer

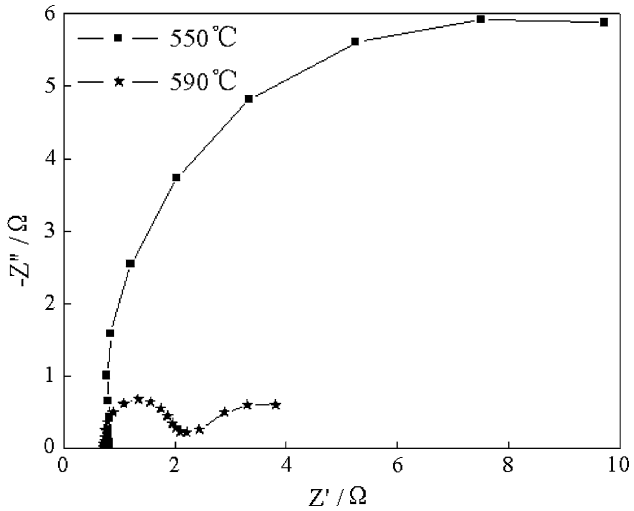

Fig. 12 AC complex impedance plots of the PEN without the graded layer

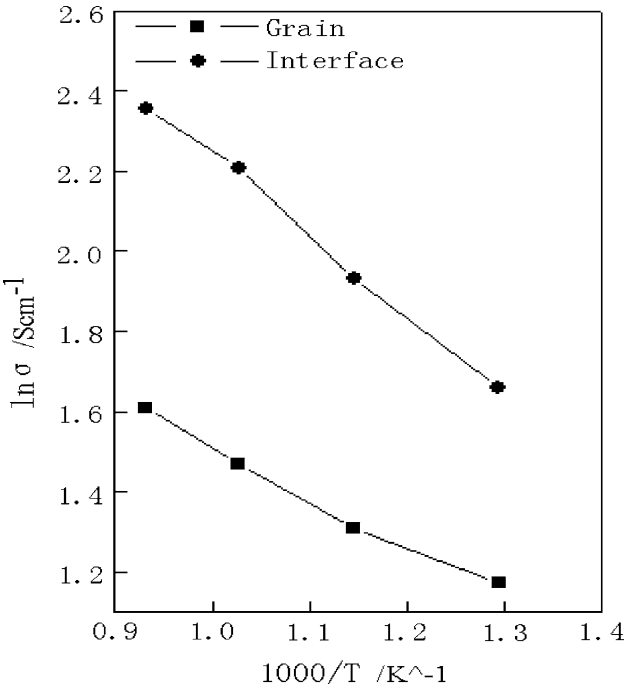

Fig. 13 Arrhenius curve of the electrical conductivity vs. temperature of the PEN with the graded layers

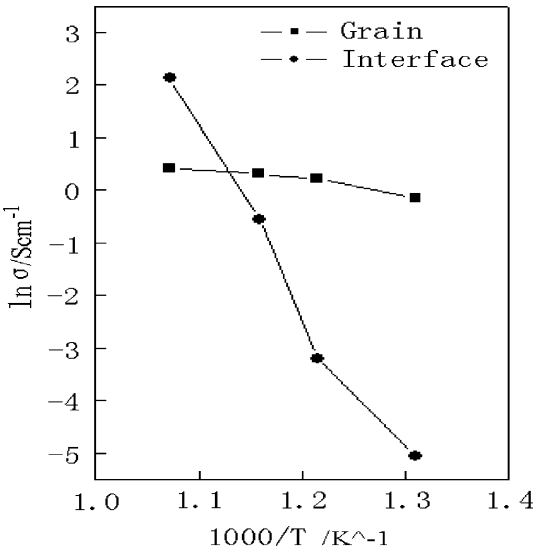

Fig. 14 Arrhenius curve of the electrical conductivity versus temperature of PEN without the graded layers

As shown in Fig. 13 and 14, in the testing temperature range, logarithmic conductivities (ln σ) of the two composite electrodes vary linearly with $1/T$. With the increase in testing temperatures, the grain resistance and the interface contact resistance decrease. In particular, the interface resistance of the composite electrode with the graded layer is far less than that of the composite electrode without the graded layer. Because the material and microstructure of the interface between the electrolyte and the graded layer and the interface between the graded layer and the cathode were not obvious, and the composition in the graded layers gradually change from the cathode to the electrolyte, the conductivity of the composite electrode gradually changes from the cathode to the electrolyte through the graded layer. However, due to the obvious variation of the material components and microstructure, the interface resistance of the composite electrode without the graded layer increased sharply.

4. Summary and Conclusions

Using a specially developed three-hopper powder feeding system, the graded functional planar and MOLB type PEN cells were fabricated by APS. Following the adjustment of the spray parameters and the addition of carbon powder into the anode powder, the porosities of the anode and the cathode were 32.74 and 32.24%, respectively, and the porosity of the electrolyte was less than 3%, which is sufficient to the operating requirements of SOFCs. The composition and microstructure of the PEN gradually vary, and the thicknesses of the graded layers were controlled in the range of ~20 to 30 μm. According to the AC complex analysis results and comparison with the electrical conductivity of the MOLB type PEN without the graded layers, the electrical conductivity of the MOLB type PEN with the graded layers increased sharply.

Acknowledgment

The authors gratefully acknowledge the contribution of the National Nature Science Foundation of China under project No. 50675081. And thanks to all who contributed in the cooperation in their experimental part. In particular, thanks to contribution of the Huazhong University of Science & Technology Analytical and Testing Center.

References

1. S.C. Singhal, Advance in Solid Oxide Fuel Cell Technology, *Solid State Ionics*, 2000, **135**(1-4), p 305-313
2. S.C. Singhal, Solid Oxide Fuel Cells for Stationary, Mobile and Military Applications, *Solid State Ionics*, 2002, **152-153**(12), p 405-410
3. B. Godfrey, K. Foger, R. Gillespie, R. Bolden, and S.P.S. Badwal, Planar Solid Oxide Fuel Cells: the Australian Experience and Outlook, *J. Power Sources*, 2000, **86**(1-2), p 68-73
4. H. Yakable, Y. Baba, T. Sakurai, and Y. Yoshitaka, Evaluation of the Residual Stress for Anode-Supported SOFCs, *J. Power Sources*, 2004, **135**(1-2), p 9-16
5. A. Moro, Y. Kuroda, and K. Kusaka, Development Status of the Reusable High-Performance Engine with Functionally Graded Materials, *Acta Astronaut.*, 2002, **50**(7), p 427-432
6. S. Turteltaub, Functionally Graded Materials for Prescribed Field Evolution, *Comput. Meth. Appl. Mech. Eng.*, 2002, **191**(21-22), p 2283-2296
7. V.E. Korepanov, The Modern Trends in Space Electro- magnetic Instrumentation, *Adv. Space Res.*, 2003, **32**(3), p 401-406
8. M.L. Pines and H.A. Bruck, Pressureless Sintering of Particle-Reinforced Metal-Ceramic Composites for Functionally Graded Materials: Part I. Porosity Reduction Models, *Acta Mater.*, 2006, **54**(6), p 1457-1465

9. Y.A. Song and S. Park, Experimental Investigations into Rapid Prototyping of Composites by Novel Hybrid Deposition Process, *J. Mater. Process. Technol.*, 2006, **171**(1), p 35-40
10. A. Yakovlev, E. Trunova, D. Grevey, M. Pilloz, and L. Smurov, Laser-Assisted Direct Manufacturing of Functionally Graded 3D Objects, *Surf. Coat. Technol.*, 2005, **190**(1-3), p 15-24
11. V. Cannillo, L. Lusvarghi, T. Manfredini, M. Montorsi, C. Siligardi, and A. Sola, Glass-Ceramic Functionally Graded Materials Produced with Different Methods, *J. Europ. Ceram. Soc.*, 2007, **27**(2-3), p 1293-129
12. B. Kieback, A. Neubrans, and H. Riedel, Processing Techniques for Functionally Graded Materials, *Mater. Sci. Eng.*, 2003, **362**(1-2), p 81-105
13. D. Hathiramani, R. Vasharpen, D. Stover, and R.J. Damani, Comparison of Atmospheric Plasma Sprayed Anode Layers for SOFCs Using Different Feedstock, *J Therm. Spray Technol.*, 2006, **15**(4), p 593-597
14. C. Zhang, H.L. Liao, W.Y. Li, G. Zhang, C. Coddet, C.J. Li, C.X. Li, and X.J. Ning, Characterization of YSZ Solid Oxide Fuel Cells Electrolyte Deposited by Atmospheric Plasma Spraying and Low Pressure Plasma Spraying, *J. Therm. Spray Technol.*, 2006, **15**(4), p 598-603
15. H. Weckmann, A. Syed, Z. Ilhan, and J. Arnold, Development of Porous Anode Layers for the Solid Oxide Fuel Cell by Plasma Spraying, *J. Therm. Spray Technol.*, 2006, **15**(4), p 604-609
16. A.A. Syed, Z. Ilhan, J. Arnold, G. Schiller, and H. Weckmann, Improving Plasma-Sprayed Yttria-Stabilized Zirconia Coatings for Solid Oxide Fuel Cell Electrolytes, *J. Therm. Spray Technol.*, 2006, **15**(4), p 617-622
17. R. Rampon, F.L. Toma, G. Bertrand, and C. Coddet, Liquid Plasma Sprayed Coatings of Yttria-Stabilized Zirconia for SOFC Electrolytes, *J. Therm. Spray Technol.*, 2006, **15**(4), p 682-688
18. R.H. Henne, T. Franco, and R. Ruckdaschel, High-Velocity DC-VPS for Diffusion and Protecting Barrier Layers in Solid Oxide Fuel Cells (SOFCs), *J. Therm. Spray Technol.*, 2006, **15**(4), p 695-700
19. D. Bouchard, L. Sun, F. Gitzhofer, and G.M. Brisard, Synthesis and Characterization of $La_{0.8}Sr_{0.2}MO_{3-\delta}$ (M = Mn, Fe, or Co) Cathode Materials by Induction Plasma Technology, *J. Therm. Spray Technol.*, 2006, **15**(1), p 37-45
20. X.Q. Ma, H. Zhang, J. Dai, J. Roth, R. Hui, T.D. Xiao, and D.E. Reisner, Intermediate Temperature Solid Oxide Fuel Cell Based on Fully Integrated Plasma-Sprayed Components, *J. Therm. Spray Technol.*, 2005, **14**(1), p 61-66
21. K.H. Shin, H. Natu, D. Dutta, and J. Mazumder, A Method for the Design and Fabrication of Heterogeneous Objects, *Mater. Des.*, 2003, **24**(5), p 339-353
22. H.O. Zhang, C.W. Jiang, G.L. Wang, and W. Wang, Membrane Electrode Assembly of Solid Oxide Fuel Cell Fabricated by Air Plasma Spray, *Funct. Mater.*, 2005, **37**(4), p 573-575, in Chinese
23. H.O. Zhang, G.L. Wang, Y.H. Luo, and T. Nakagawa, Rapid Hard Tooling by Plasma Spraying for Injection Molding and Sheet Metal Forming, *Thin Solid Films*, 2001, **390**(1), p 13-19
24. A. Momma, Y. Kaga, K. Takano, K. Nozarka, and A. Negishi, AC Impedance Behaviour of a Practical-Size Single-Cell SOFC under DC Current, *Solid State Ionics*, 2004, **174**(1-4), p 87-95
25. H.K. Lee, Electrochemical Characteristics of $La_{1-x}Sr_xMnO_3$ for Solid Oxide Fuel Cell, *Mater. Chem. Phys.*, 2002, **77**(3), p 639-646